Rotating Stars from *Kepler* Observed with Gaia DR2

JAMES. R. A. DAVENPORT[1, 2, *] AND KEVIN R. COVEY[1]

[1]*Department of Physics & Astronomy, Western Washington University, 516 High St., Bellingham, WA 98225, USA*
[2]*Department of Astronomy, University of Washington, Seattle, WA 98195, USA*

ABSTRACT

We have matched the astrometric data from *Gaia* Data Release 2 to the sample of stars with measured rotation periods from *Kepler*. Using 30,305 stars with good distance estimates, we select 16,248 as being likely main sequence single stars centered within a 0.5 mag region about a 1 Gyr isochrone, removing many sub-giants and unresolved binary stars from the sample. The rotation period bimodality, originally discovered by McQuillan et al. (2013), is recovered for stars out to 525pc, but is not detectable at further distances. This bimodality correlates with Galactic height as well, dropping strongly for stars above $Z > 90$ pc We also find a significant width in the stellar main sequence of $M_G \sim 0.25$ mag, as well as an increase in the average rotation period correlated with the M_G offset at a given color (mass). We interpret this to be the measurable change in luminosity and loss of angular momentum as stars evolve along the main sequence, which may provide a new independent test of both stellar evolution and gyrochronlogy models.

1. INTRODUCTION

The *Kepler* mission (Borucki et al. 2010), through its unmatched combination of photometric precision and years-long observation baseline, has produced the largest sample of rotating stars to date. Stellar rotation has long been noted as a means to possibly age-date stars due to their constant angular momentum loss via winds (Skumanich 1972). While studies of open clusters give hope that this "gyrochronology" model broadly works for solar-type and lower-mass stars, many uncertainties exist about the details of this spin-down and its utility as a clock. These include questions about the initial rotation period distribution for stars (e.g. Barnes 2010; Matt et al. 2015), the specific analytic prescription for modeling the spin-down (Angus et al. 2015), and exploring the efficiency of this angular momentum loss mechanism at older ages (van Saders et al. 2016).

One of the most compelling results from the rotating star sample in *Kepler* is the discovery of a bimodal period distribution. McQuillan et al. (2013) first found a bimodality in the distribution of field M dwarfs with periods between ∼10 and ∼50 days. This feature was also found in the *Kepler* field K dwarfs in (McQuillan et al. 2014). Using Gaia DR1, Davenport (2017) was able to remove contaminating subgiants from the rotation sample and found the bimodality extended to the G dwarfs as well. This bimodal rotation period distribution is ei-

Corresponding author: James. R. A. Davenport
James.Davenport@wwu.edu

* NSF Astronomy and Astrophysics Postdoctoral Fellow
  DIRAC Fellow

ther a new short-lived transition or instability phase of angular momentum loss, or a signature of star formation history imprinted in the present-day rotation period distribution. However, to date this feature has only been observed in the *Kepler* rotation period catalog, and most critically only for stars within ∼300 pc.

In this paper we follow the work of Davenport (2017) in refining the *Kepler* rotation period sample using astrometric data from the *Gaia* mission (Gaia Collaboration et al. 2016). By matching the McQuillan et al. (2014) rotation period catalog to the newest data from *Gaia* Data Release 2 (Gaia Collaboration et al. 2018), we can use precise distances for essentially every star to select the most-likely main sequence dwarfs to distances well over 1 kpc. Importantly this filters out both sub-giants, the main contaminant noted by Davenport (2017), and unresolved binary stars. Here we demonstrate the power of such a combined time-domain and astrometric sample for constraining the detailed evolution of main sequence stars themselves, and exploring the star formation history of the Milky Way.

2. THE *Kepler*–GAIA DATA

We used the largest homogeneous catalog of rotation periods available from the *Kepler* mission. The sample from McQuillan et al. (2014) provides rotation periods for more 34,030 stars, measured using the Auto-Correlation Function (ACF). While the ACF does not have as fine of resolution in recovering periods as compared with methods such as the Lomb-Scargle Periodogram, it is more robust to detecting the true period as opposed to an alias, and more complete for batch analysis of all stars (e.g. see Aigrain et al. 2015).

The *Kepler* data was matched to the *Gaia* DR2 source catalog using a 1 arcsecond radius. We used the *Kepler*–Gaia cross-match made publicly available by M. Bedell, which included entries for 195,830 sources. *Kepler*-based stellar

parameters included in this cross-match come the Data Release 25 *Kepler* catalog. Joining this cross-matched table to the McQuillan et al. (2014) catalog, we found 33,538 sources.

To select stars with good parallaxes, as well as high quality photometry from *Gaia*, we selected stars with the following criteria:

- Parallax error < 0.1 mas

- $\sigma(M_G)/M_G < 0.01$

- $\sigma(G_{BP})/G_{BP} < 0.01$

- $\sigma(G_{RP})/G_{RP} < 0.01$

Rather than simply use the inverse *Gaia* parallax values to measure the distance to sources, we use the improved distance prescription from Bailer-Jones et al. (2018), who provided independent distances estimates for 1.33 billion *Gaia* sources using a weak prior on the distribution of stars in our galaxy. We follow their suggested use of the distance catalog, we only include sources with `modality_flag ==` 1 (i.e. not a bimodal distance solution) and `result_flag == 1` (i.e. a well constrained distance).

Our final sample contained 30,305 stars in *Gaia* DR2 with measured *Kepler* rotation periods that passed these selection criteria. A color–magnitude diagram (CMD) of this sample using the *Gaia* bands is presented in Figure 1, with points colored by their measured *Kepler* rotation periods.

3. SELECTING MAIN SEQUENCE STARS

As in Davenport (2017), the color–magnitude diagram in Figure 1 shows many of the bluer stars in the McQuillan et al. (2014) sample are located significantly above the main sequence. These are likely subgiant stars, which do not follow the main sequence stars spin-down evolution (e.g. do Nascimento et al. 2012; van Saders & Pinsonneault 2013). Since Davenport (2017)
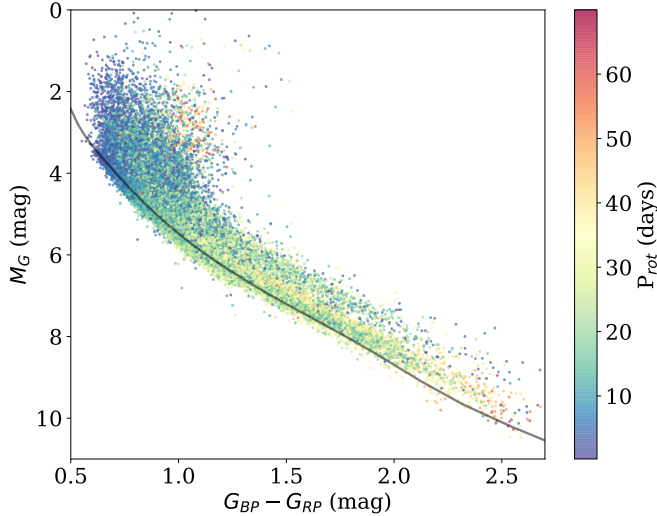
Figure 1. Color–magnitude diagram for 30,305 *Kepler* stars from the McQuillan et al. (2014) sample that are included in *Gaia* DR2, colored by their measured rotation period. For reference we show a 10^9 year MIST isochrone (black line) used to select likely main sequence, single stars (black line). A track of binary stars is apparent ~0.75 mag above the main sequence. As in Davenport (2017), we find significant contamination of the rotation period sample for bluer stars by sub-giants.

found subgiants could obscure the rotation period bimodality for G dwarfs, these must be excluded from our analysis, but we encourage future studies to explore the wealth of angular momentum evolution data from these most-main sequence objects.

Beyond the subgiant contamination, we also see a secondary population of stars in a parallel track ~0.75 mag above the normal main sequence, which are attributed to unresolved binary star systems. This pile-up above the main sequence occurs due to unresolved equal-mass (or nearly equal-mass) field binaries, and was seen in the *Gaia* DR1 data as well (Anderson et al. 2017). Since these systems may have experienced tidal evolution that could significantly impact their rotation evolution (e.g. Lurie et al. 2017), we must also remove these from our analysis. Though we do not explore the binary

population in any detail here, this sample (perhaps with radial velocity follow-up) may provide useful insight into the tidal evolution of binary stars, and are good targets for characterizing binary star system properties. We also note a small number of systems above the even the equal-mass binary main sequence track, which could be due to unresolved triple star systems.

We use an isochrone from the Mesa Isochrones and Stellar Tracks suite (MIST; Choi et al. 2016) to choose likely main sequence stars in Figure 1. Our favored model to represent the main sequence in this study had [Fe/H] = +0.25 and an age of 10^9 years, and was chosen by hand. Single, main sequence stars were selected in a region spanning 0.1 mag fainter and 0.4 mag brighter than the MIST isochrone, resulting in a final sample of 16,248 stars for analysis of their rotation period distributions.

4. TRACING THE PERIOD BIMODALITY

Using this sample of likely single, main sequence stars from *Kepler* and *Gaia*, we are able to explore the distribution of rotation periods for stars as a function of their distance. The rotation period bimodality in *Kepler* stars previously only detected for stars within ~300 pc of the Sun due to the limits of available parallax data. Now with *Gaia* DR2, our sample of main sequence star with measured rotation periods in *Kepler* extends out to over 2 kpc.

In Figure 2 we present the period–color diagram for our sample of stars, split into six bins of projected distance. The first panel (0–350 pc) effectively reproduces the results of Davenport (2017) for bluer stars and McQuillan et al. (2014) for the redder stars. A gap in the observed rotation periods as a function of color is seen, at a period of approximately 5 days for $G_{BP} - G_{RP} \approx 1$, 20 days for $G_{BP} - G_{RP} \approx 2$, and increasing towards 30 days for the reddest stars in our sample. This gap corresponds with a line of approximately constant age, consistent
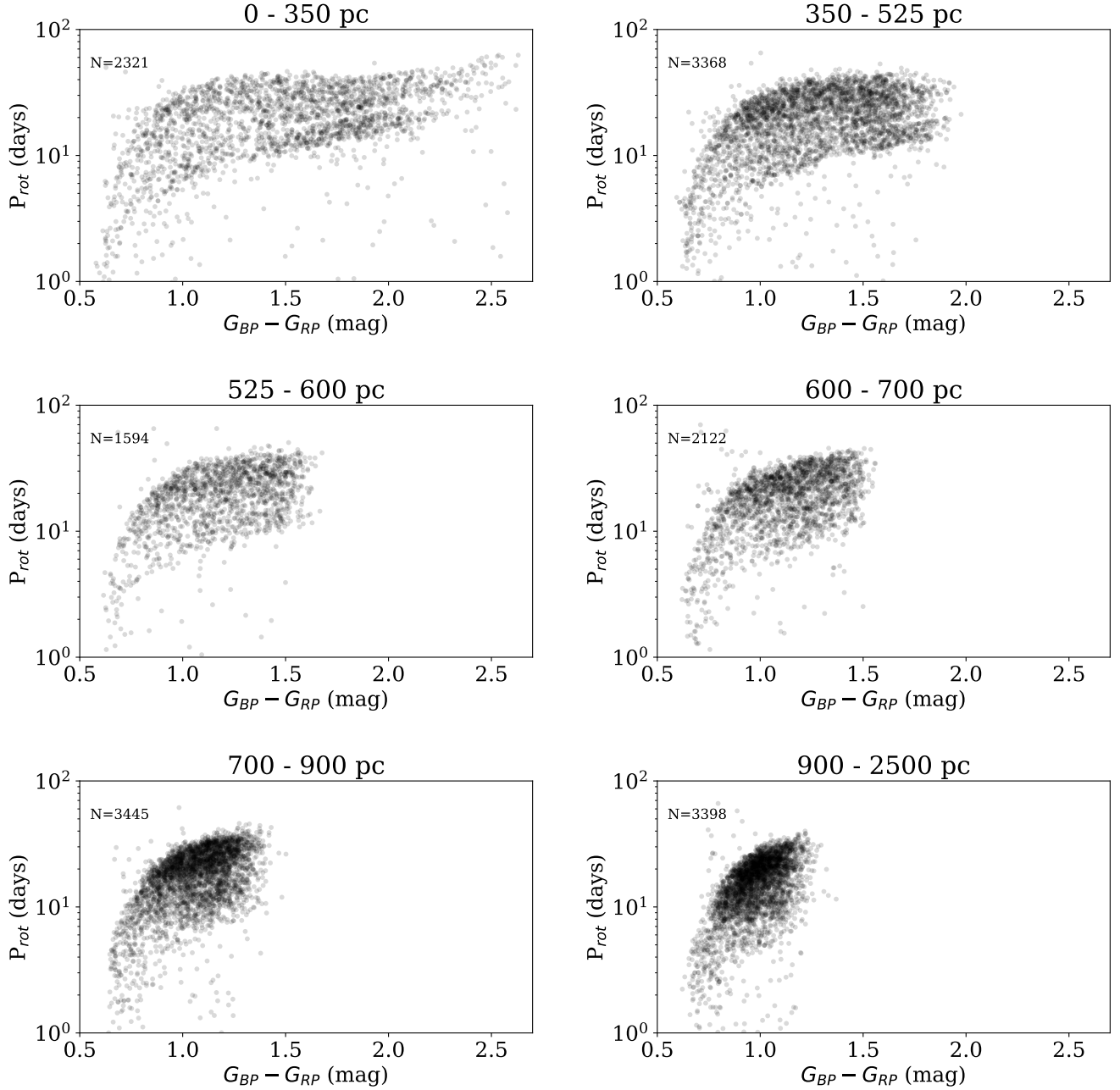
Figure 2. Color–period diagrams for our sample of likely main sequence stars, divided into six bins of distance. Our nearest bin (within 350pc) is effectively the distance analyzed in Davenport (2017) using Gaia DR1, and clearly shows the rotation period bimodality for the entire sample. The brighter magnitude limit of the *Kepler* sample results in redder (fainter) stars missing in our further distance bins. The rotation period bimodality can be seen in the 350-525 pc bin, but is not found in the bluer stars at further distances.

with a gyrochrone with age $\sim$600 Myr (Davenport 2017).

The bimodality is still apparent in the second distance bin (350–525 pc), clearly visible in the redder stars, but seems to fade in the final three bins. Other structures in the period distributions are visible, however. For example, a thin sequence of stars with rotation periods near 10 days is faintly visible in the most distant bin (900–2500 pc) for stars with colors of $0.8 < G_{BP} - G_{RP} < 1.2$. This feature is due to the 1 Gyr open cluster NGC 6811 in the *Kepler* field (Meibom et al. 2011), whose distance is $\sim$1100 pc (Sandquist et al. 2016).

To better illustrate the evolution of rotation periods for all the stars between the distance bins, in Figure 3 we follow Davenport (2017) and subtract the rotation period of a 600 Myr gyrochrone. As no published gyrochronology model yet exists that has been tuned to the *Gaia* photometric colors, we adopt the same gyrochronology model of Eqn. 2 from Meibom et al. (2009) used by Davenport (2017) to approximately trace the rotation period gap at 600 Myr as a function of $B - V$ color. We convert stars from the observed *Gaia* $G_{BP} - G_{RP}$ color to $B - V$ using the same 1 Gyr MIST isochrone model used to define the main sequence in Figure 1 above.

Our sample naturally becomes biased towards the bluer (brighter) stars as we reach larger distances. Since bluer stars have more rapid rotation and more dramatic period evolution, gyrochronology models are "bent" strongly for these stars, and thus the period bimodality (or other structures) become difficult to distinguish. Davenport (2017) used an ad-hoc modification of the gyrochrone model for the hottest stars to illustrate the existence of the period bimodality. However, in Figure 3 we limit our analysis to stars with $0.8 < B - V < 1.5$ (approximately $0.9 < G_{BP} - G_{RP} < 2.2$, or $0.9 > M_\odot > 0.5$), where the gyrochrone is most flat as a function of color. This color range was chosen to ensure ample stars were available in each distance bin, but without having to use the ad-hoc gyrochrone model correction from Davenport (2017).

Figure 3 (left) shows clearly that for the short period component of the rotation period bimodality dominates only for the nearest stars, and steadily decreases with increasing distance. The *Kepler* field is centered on a Galactic latitude of $b \sim 13.5°$, and so we can also study the period bimodality as a function of height above the Galactic mid-plane. Both galaxy formation simulations (Ma et al. 2017) and observations of stars in the nearby Milky Way (Xiang et al. 2017) indicate that height above the mid-plane correlates strongly with the median ages for stars, out to distances of several kpc. The Milky Way thin disk has a scaleheight of $\sim$300 pc (Gilmore & Reid 1983). However, since the *Kepler* field is oriented towards low latitudes we do not reach significant *heights* above the disk. The projected height above the mid-plane for the distance bins shown in Figures 2 and 3 ranges from $Z \sim 100$ pc at a distance of $d = 350$ pc to $Z \sim 230$ pc at $d = 900$ pc. As a result, we are only sensitive to changes in the youngest stars within this span of Z.

In Figure 3 (right) we find that the drop-off of the short-period (rapid rotating) component of the period bimodality is even more pronounced as a function of Z, decreasing rapidly after only 90 pc. With increasing height we also see that the shift to the longer period component is more smooth. However, from these two projections in Figure 3 alone (distance and height) we cannot definitively determine the spatial structure of the rotation period bimodality.

As a first attempt at understanding the spatial extent of this age-related feature, in Figure 4 we break the lowest height stars ($Z < 100$ pc) in to two roughly even samples, split as a function of their projected distance. Note we have
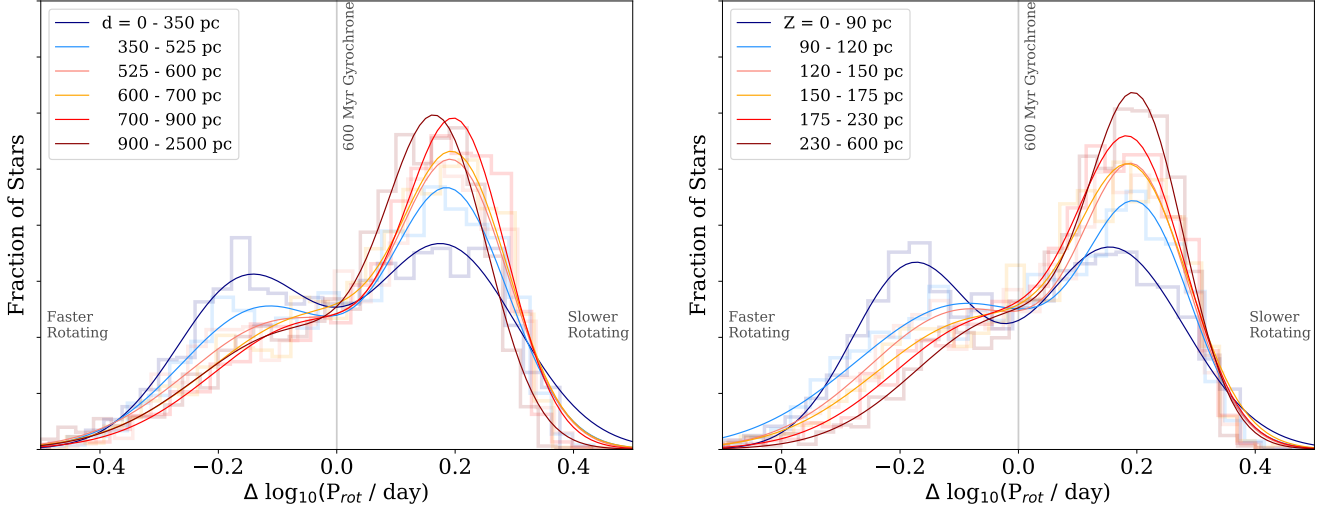
Figure 3. Left: Distribution of the log rotation periods after a 600 Myr gyrochrone was subtracted, using the same distance bins shown in Figure 2 (faint lines). Two-gaussian models were fit to each histogram (bold lines). The rotation period bimodality for stars within 350 pc has two nearly equal peaks similar to those found in Davenport (2017), at -0.15 and +0.18 dex. The fast rotating peak (left side) declines sharply at further distances. Right: Same as Left, but in bins of Galactic height above the plane (Z). The drop-off of fast rotating, young stars is even more pronounced as a function of height.

also repeated this exercise for stars in higher ranges of Z, and find the decline of the rapid rotators is again uniform between subsamples of varying projected distance. The rotation period bimodality is clearly seen in both distance bins of Figure 4, indicating that the feature is likely not a localized star formation history artifact centered around the Sun. Instead, we believe this feature is characteristic of the age–Z dynamical correlation observed within the solar neighborhood of our Galaxy.

5. RECALIBRATING STELLAR EVOLUTION MODELS

A subtle feature we noticed in Figure 1 is the color gradient (i.e. rotation period gradient) for the stars in between the single and binary star main sequence populations. In Figure 1 this appears as a yellow stripe (i.e. rotation periods of 30-40 days) between these blue-green sequences for systems with colors of $G_{BP} - G_{RP} \approx 1.5$. To exaggerate this feature, we have reproduced a portion of our color–magnitude diagram focused on the main sequence near this stellar color in

the left panel of Figure 5. A clear color gradient is present, with red points (slower rotators) appearing preferentially above the main sequence. The right panel of Figure 5 concretely demonstrates a correlation between the measured rotation period and the vertical offset (i.e. absolute magnitude) from the 10^9 year MIST isochrone. Slower rotating stars are brighter at a given color.

We interpret this observation as being due to the increase in luminosity of stars across their main sequence lives, coupled with the angular momentum loss that underpins gyrochronology. Indeed, the three MIST isochrones shown in Figure 5 with ages of 10^8, 10^9, and 10^{10} years clearly predicts a net increase in brightness of the main sequence over time. We also track the color–magnitude evolution of a 0.7 $M_\odot$ star over its lifetime in Figure 5, which shows the "hook" the star takes over its main sequence life.

Inverting the color–magnitude diagram into precise ages for main sequence stars using *Gaia* is beyond scope of this work. However, Fig-
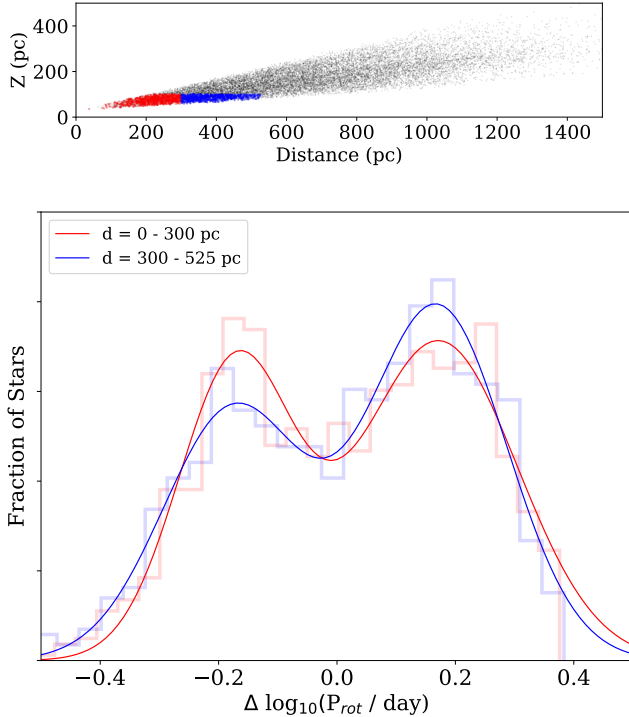
Figure 4. Top: projected distance and Galactic height of the main sequence stars in our sample. Two approximately equal subsets of stars near the Galactic mid-plane have been highlighted, those with distances from the sun of $d < 300$ pc (red), and with $300 < d < 525$ pc. Bottom: As in Figure 3, the distribution of rotation periods after a 600 Myr gyrochrone was subtracted (faint lines), and with two-Gaussian fits (bold lines) for the same subsets of stars as above. The period bidmodality is seen in both distance bins, suggesting it is not localized around the Sun.

ure 5 clearly demonstrates that age information is not only present in the CMD for main sequence stars, but it may also be a larger amplitude effect than previously assumed. For example: younger, presumably more metal rich stars, should have redder main sequence colors. This in turn should move the entire main sequence track to the right in the CMD. However, we find older stars (slower rotators) appearing on the right side of the main sequence, due to their increased luminosity with age. The main sequence location of a star is therefore not simply

due to its mass and metallicity in the *Gaia* era, but its age must also be taken into account.

In Figure 5 we also show the change in brightness as a function of the rotation period for the stars in our zoomed-in CMD, as well as a prediction for the evolution of a 0.7 $M_\odot$ star. The spin-down model here is a combination of the MIST isochrone evolution, as well as the Meibom et al. (2009) gyrochronology model. Note this spin-down model has been arbitrarily offset in the ΔM_G to roughly go through the observed data at the rapid rotation end. While *Kepler* light curves generally are not able to measure rotation periods reliably with periods longer than 20 or 30 days, we find that stars with brightness (vertical) offsets in the CMD consistent with being several Gyr old have average rotation periods far shorter than the 60–80 days values predicted from the spin-down models.

One interpretation of this result may be that the older stars are spinning *faster* than expected for stars their age. This is qualitatively similar to the model of broken spin-down occurring at a critical Rossby number suggested by van Saders et al. (2016). Though we cannot definitively confirm such intriguing rotation evolution from this initial investigation given the observation bias for long periods from *Kepler*, matching the *Gaia* CMD with other rotation period measurements may provide an ideal dataset to test the van Saders et al. (2016) model against. The ability to simultaneously constrain the precise CMD location and surface rotation rate, as with the sample demonstrated here, may also be a valuable method for calibrating a new generation of isochrone and gyrochronology models.

6. DISCUSSION

we find period bimodality is localized to low galactic heights, not only close distances to the Sun. using rotation to trace the ages of nearby stars. would be really neat to compare the spatial structure of star formation in detail, as
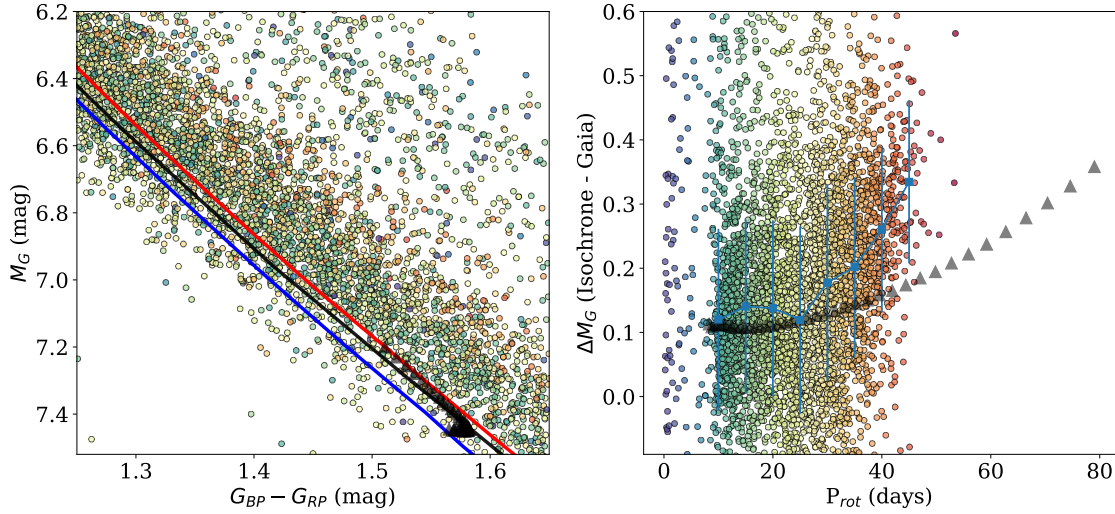
Figure 5. Left: Enlarged portion of the color–magnitude diagram from Figure 1 in a region centered near ~ 0.75 M$_\odot$, with stars are colored by their measured *Kepler* rotation periods from McQuillan et al. (2014). MIST isochrones at ages of 10^8, 10^9, and 10^{10} yr are shown for comparison (blue, black, and red lines). The predicted evolution of a 0.7 M$_\odot$ star is highlighted (black triangles). Right: Difference in M_G from the 10^9 yr MIST isochrone as a function of rotation period (point color again indicates rotation period, as in Left panel). Blue squares show an increase in the median M_G offset in bins of increasing rotation period. Error bars shown are the standard deviation of ΔM_G in each bin. The 0.7 M$_\odot$ star brightness evolution is shown as a function of rotation evolution from Meibom et al. (2009) (black triangles).

Lewis et al. (2015) for example show lots of variation in SFH in 100pc bins for M31 and find out what the actual extent/coherence of the bimodality is.

Adding to the sample of rotation periods from Kepler using K2 (Foreman-Mackey in prep?), not only for doubling the sample size to investigate trends with more precision, but also the wider range of galactic fields of view mean wider range of ages/SFH's we can sample.

We note a shortcoming of our approach in normalizing the rotation period distributions to a 600 Myr gyrochrone in Figure 3 is that it gives the false appearance that this age is a universal transition point. A more robust approach is needed that uses improved gyrochronology models to invert the observed color–period diagrams into age distributions.

finally, this work has found strong motivation for a new generation of gyrochronology isochrones to adequately model the *Gaia–Kepler*/K2 (and soon TESS) rotation data for field stars. As we show in Figure 5, these models should include both the angular momentum evolution (period), as well as the temperature and luminosity (color, magnitude) as a function of time. With such improvements, we may be able to

REFERENCES

Aigrain, S., Llama, J., Ceillier, T., et al. 2015, MNRAS, 450, 3211, doi: 10.1093/mnras/stv853

Anderson, L., Hogg, D. W., Leistedt, B., Price-Whelan, A. M., & Bovy, J. 2017, ArXiv e-prints. https://arxiv.org/abs/1706.05055

Angus, R., Aigrain, S., Foreman-Mackey, D., & McQuillan, A. 2015, MNRAS, 450, 1787, doi: 10.1093/mnras/stv423

Bailer-Jones, C. A. L., Rybizki, J., Fouesneau, M., Mantelet, G., & Andrae, R. 2018, ArXiv e-prints. https://arxiv.org/abs/1804.10121

Barnes, S. A. 2010, ApJ, 722, 222, doi: 10.1088/0004-637X/722/1/222

Borucki, W. J., Koch, D., Basri, G., et al. 2010, Science, 327, 977, doi: 10.1126/science.1185402

Choi, J., Dotter, A., Conroy, C., et al. 2016, ApJ, 823, 102, doi: 10.3847/0004-637X/823/2/102

Davenport, J. R. A. 2017, ApJ, 835, 16, doi: 10.3847/1538-4357/835/1/16

do Nascimento, J.-D., da Costa, J. S., & Castro, M. 2012, A&A, 548, L1, doi: 10.1051/0004-6361/201219791

Gaia Collaboration, Brown, A. G. A., Vallenari, A., et al. 2018, ArXiv e-prints. https://arxiv.org/abs/1804.09365

Gaia Collaboration, Prusti, T., de Bruijne, J. H. J., et al. 2016, A&A, 595, A1, doi: 10.1051/0004-6361/201629272

Gilmore, G., & Reid, N. 1983, MNRAS, 202, 1025, doi: 10.1093/mnras/202.4.1025

Lewis, A. R., Dolphin, A. E., Dalcanton, J. J., et al. 2015, ApJ, 805, 183, doi: 10.1088/0004-637X/805/2/183

Lurie, J. C., Vyhmeister, K., Hawley, S. L., et al. 2017, AJ, 154, 250, doi: 10.3847/1538-3881/aa974d

Ma, X., Hopkins, P. F., Wetzel, A. R., et al. 2017, MNRAS, 467, 2430, doi: 10.1093/mnras/stx273

Matt, S. P., Brun, A. S., Baraffe, I., Bouvier, J., & Chabrier, G. 2015, ApJL, 799, L23, doi: 10.1088/2041-8205/799/2/L23

McQuillan, A., Aigrain, S., & Mazeh, T. 2013, MNRAS, 432, 1203, doi: 10.1093/mnras/stt536

McQuillan, A., Mazeh, T., & Aigrain, S. 2014, ApJS, 211, 24, doi: 10.1088/0067-0049/211/2/24

Meibom, S., Mathieu, R. D., & Stassun, K. G. 2009, ApJ, 695, 679, doi: 10.1088/0004-637X/695/1/679

Meibom, S., Barnes, S. A., Latham, D. W., et al. 2011, ApJL, 733, L9, doi: 10.1088/2041-8205/733/1/L9

Sandquist, E. L., Jessen-Hansen, J., Shetrone, M. D., et al. 2016, ApJ, 831, 11, doi: 10.3847/0004-637X/831/1/11

Skumanich, A. 1972, ApJ, 171, 565, doi: 10.1086/151310

van Saders, J. L., Ceillier, T., Metcalfe, T. S., et al. 2016, Nature, 529, 181, doi: 10.1038/nature16168

van Saders, J. L., & Pinsonneault, M. H. 2013, ApJ, 776, 67, doi: 10.1088/0004-637X/776/2/67

Xiang, M., Liu, X., Shi, J., et al. 2017, ApJS, 232, 2, doi: 10.3847/1538-4365/aa80e4